International Symposium
On Turbulence and Shear Flow
Phenomena (TSFP-9)
June 30 - July 3, 2015 *Melbourne, Australia*

THE EFFECT OF REFERENCE FRAME SELECTION ON MODELLED TURBULENCE FOR GROUND EFFECT AERODYNAMICS SIMULATIONS

Tracie Barber
School of Mechanical Engineering
University of New South Wales
NSW 2052 Australia
t.barber@unsw.edu.au

James Keogh
School of Mechanical Engineering
University of New South Wales
NSW 2052 Australia
j.keogh@unsw.edu.au

John Reizes
School of Mechanical Engineering
University of New South Wales
NSW 2052 Australia
j.reizes@unsw.edu.au

ABSTRACT

The principle of aerodynamic reciprocity is foundational in the study of fluid mechanics. A wind tunnel framework is generally used to test aerodynamic performance and this body-stationary convention has continued into the computational regime. However, there is no practical reason why the moving body/stationary fluid situation that corresponds to reality cannot be used for computational modelling. When the concept of ground effect aerodynamics is studied, an extra boundary is required which must move, and the extra boundary condition also adds complexity to a computational simulation. The introduction of freestream turbulence, as well as possible additional turbulent generation from the moving ground, raise the possibility of spurious turbulent values, particularly when calculated using a RANS based closure in a CFD model. Here, a ground effect aerodynamics study is undertaken computationally, using a body-stationary and a body-moving reference frame, to examine any variation that occurs. Two models for turbulence are implemented, the Realizable k-ε model and the Reynolds Stress Model (RSM).

INTRODUCTION

Ground effect aerodynamics, in which a lifting surface operates in close proximity to the ground, has relevance to aircraft landing and takeoff, automotive operations (especially high-speed racing conditions) and also to the design and operation of wing in ground vehicles, or ekranoplans. Simulations of ground effect aerodynamics are somewhat complicated by the need for a moving ground, if a body-fixed reference frame is used - standard for most aerodynamic investigations. Experimentally, this involves the construction and careful implementation of a conveyor system on the lower floor of the wind tunnel (Diasinos *et al.*, 2005), while computationally the implementation of a moving ground is relatively straightforward. For a computational solution, the accurate and appropriate specification of boundary conditions is an important part of the solution process and only the ground moving condition accurately simulates ground effect aerodynamics (Barber *et al.*, 1999) (however studies still occur where stationary ground models are used (Pillai *et al.*, 2014)).

In general, for lifting wings near the ground, increased lift and increased lift to drag ratio when approaching the ground are found (Ahmed *et al.*, 2007). Early work in the field of ground effect frequently made use of incorrect boundary conditions on the ground, leading to considerable confusion around the mechanisms causing the change in aerodynamics performance (Barber *et al.*, 2002). Previous work exclusively utilises body-stationary approaches for both experimental and computational analyses.

The use of a body-stationary reference frame is the most commonly used system of aerodynamic simulation (though not necessarily in naval architecture where towing tanks are common), using either a body-fixed wind tunnel or body-fixed CFD situation to simulate the real-life case of a body moving through a fluid. This principle of aerodynamic reciprocity was defined in the 16th century, when Da Vinci proposed that fluid flow is the same whether the body moves through a medium at a given velocity or the medium flows past the stationary body at the same velocity (Giacomelli, 1930). While the methodology is well-accepted, the widespread commonality of the body-fixed solution and the subsequent explanation of the flow features based on the flow characteristics seen in this reference frame could be problematic in certain cases. In particular, when the situation being examined includes another boundary, which also must be taken into a different reference frame (such as in ground effect aerodynamics), the body-fixed explanations may obscure the true nature of the flow regime (Close & Barber, 2014). The explanation of such characteristics cause confusion to those unfamiliar with the change in reference frame, and in some cases the cause and effect of the flow properties may be improperly or poorly explained.

A further consideration relates to the possible introduc-

tion of greater levels of turbulence into the flow field, due to a moving surface on the ground boundary. Reducing levels of free-stream turbulence (or often simply unsteadiness), is a well-known component to wind tunnel design. In a moving ground wind tunnel, the free-stream air and additionally, the lower surface of the wind tunnel are moving, and potentially turbulent generators. The use of RANS turbulence closures may also contribute further numerical error in their treatment of the generation terms for these moving surfaces.

While more sophisticated models for turbulence such as DES and LES are increasingly seeing use in the study of ground effect aerodynamics, RANS models are still commonplace, and particularly the use of eddy-viscosity based models (Qu *et al.*, 2015; Doig *et al.*, 2014; Lee & Lee, 2013; Qu *et al.*, 2014).

The purpose of this study is to re-examine ground effect in both a body-stationary reference frame and a body-moving reference frame to determine if any discrepancies may occur.

METHODOLOGY

Two three-dimensional models are developed: the first is called "stationary", indicating that the airfoil is stationary with the fluid moving past it, and the second is called "moving", indicating that the airfoil is moving in a still atmosphere. It is possible to simulate a stationary flow field by using a moving reference frame model. Although intended for use in turbomachinery studies for rotor-stator interaction, the constant velocity of an airfoil moving through stationary air is simulated by implementing a steady velocity of the coordinate system attached to the wing. The main variation is that rather than using the absolute velocity, the relative velocity is employed in the conservation equations and it is given by

$$\widetilde{V}_r = \widetilde{V} - \widetilde{V}_t \tag{1}$$

in which $\widetilde{V}_t$ is the translational velocity of the frame of reference attached to the airfoil, so the equations of continuity and momentum are then written in the relative frame.

The test-case used is a computational model based on detailed experimental data obtained by Zerihan (Zerihan & Zhang, 2000). A chord length of 223.4 mm and span of 1100 mm gave an aspect ratio of 4.92, and the inverted T026 wing is studied at 3.45^o angle of incidence and a clearance of h/c (height/chord) = 0.179. Computational models are run as symmetric about the wing midspan and the freestream air conditions matched those used in the Southampton Low-Speed Wind Tunnel (Zerihan & Zhang, 2000). The pressure-based implicit coupled solver was utilised to achieve steady-state simulations. Simulations were run using a second-order node-based upwinding discretization scheme and the convergence criteria set for when aerodynamic forces ceased to change by more than 0.02% over 1000 continued iterations, and a point velocity monitor placed near the centre of the prominent lower vortex also ceased to change by more than 0.02%. The simulations were solved across 64 processors on the UNSW Australia Trentino cluster.

The calculated Reynolds number for the simulations (based on chord-length) was of $4.54\text{x}10^5$. In the experimental setup a grit strip was located at 0.1c on both the pressure and suction surfaces of the wing was used to enable transition and this was computationally modelled for the validation (further models used a fully turbulent domain). The reader is directed to our earlier work for details of this validation and the mesh refinement study (Keogh *et al.*, 2015). A multi-block, completely structured meshing technique was employed and y^+ values remained below one over the wing, endplate and ground plane. The three-dimensional mesh consisted of $7.6\text{x}10^6$ cells with 117 in the spanwise direction and and 185 in the chordwise direction. Following a boundary location sensitivity study, the downstream boundary was located at 50c, and the walls, roof and inlet at 10c from the wing.

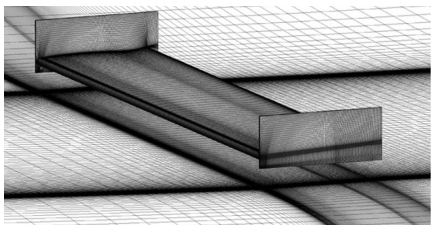

(a) isometric view of mesh

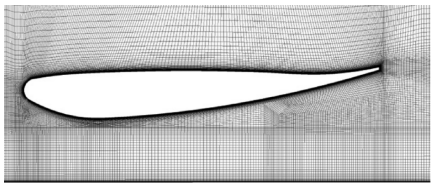

(b) mesh across the midspan of the wing

Figure 1. *Description of the mesh structure used, consisting of $7.6\text{x}10^6$ cells in a fully structured domain. The downstream boundary is located at 50c, and the walls, roof and inlet at 10c from the wing.*

For the stationary case, the upstream boundary is a velocity inlet set to 30ms^{-1} and the top and side walls of the domain are set as stationary walls without shear stress, in order to simulate an infinite boundary. The ground surface is set as a moving wall at 30m^{-1} and the downstream boundary is set as a uniform zero pressure.

In the moving case, the upstream boundary is set to a mass flow inlet (with zero flux), the downstream boundary as uniform zero pressure and the top and side walls of the domain are set as stationary walls. The ground surface is set as a moving wall with zero absolute velocity and the surface of the airfoil is treated as a solid boundary and given a velocity of -30ms^{-1} . The entire fluid zone for the moving case is also defined as a moving reference frame, being given a translational velocity of -30ms^{-1}.

The Reynolds averaged Navier Stokes (RANS) equation, as follows, is solved.

$$\rho\frac{\partial U_i}{\partial t} + \rho U_j\frac{\partial U_i}{\partial x_j} = -\frac{\partial P}{\partial x_i} + \frac{\partial}{\partial x_j}\left(2\mu S_{ji} - \overline{\rho u_j' u_i'}\right) \tag{2}$$

where $\rho\overline{u_j' u_i'}$ is the Reynolds stress tensor (often written simply as τ_{ij}). Two equation models, such as k-ε models,

make use of the Boussinesq eddy viscosity approximation to find the Reynolds stress tensor as a product of the mean strain rate tensor and an eddy viscosity. We can then represent τ_{ij} as:

$$\tau_{ij} = \mu_t S_{ij} - \frac{2}{3}\mu_t \frac{\partial u_k}{\partial x_k}\delta_{ij} \tag{3}$$

where μ_t is the turbulent viscosity and S_{ij} is the modulus of the strain rate tensor:

$$\mu_t = f_\mu \cdot C_\mu \frac{\rho k^2}{\varepsilon} \tag{4}$$

and

$$S_{ij} = \frac{\partial u_i}{\partial x_j} + \frac{\partial u_j}{\partial x_i} \tag{5}$$

The value calculated for the turbulent viscosity is dependent upon factors including the freestream turbulence intensity, solid boundaries and the flow history effect, which can persist for long distances (Wilcox *et al.*, 1998).

Two models for closure of the equations are utilised, the Realizable k-ε model and the linear pressure-strain Reynolds Stress Model (RSM) (Launder, 1989). In the standard k-ε model, the model coefficients are constant and derived from experiments; in the Realizable k-ε model, C_μ is a variable and the model now ensures positivity of the normal stresses (Shih *et al.*, 1993).

The RSM achieves closure of Equation 2 by the use of additional transport equations for the six Reynolds stresses (Launder *et al.*, 1975), and therefore avoids the use of the eddy viscosity assumption on which the k-ε models are based. It is a physically more complete model, accounting for flow history, curvature effects, turbulent transport and anisotropy of turbulent stresses.

By implementing the two types of models, with their associated levels of complexity, the effect on turbulent generation can be examined.

Table 1. Description of cases studied

Name	**Reference frame**	**Turbulence model**
A	stationary	realizable k-ε
B	stationary	RSM
C	moving	realizable k-ε
D	moving	RSM

RESULTS AND DISCUSSION

Pressure contours on the symmetry plane are presented in Figure 2, in which the expected general equivalence of the reference frames is apparent. The increase in downforce

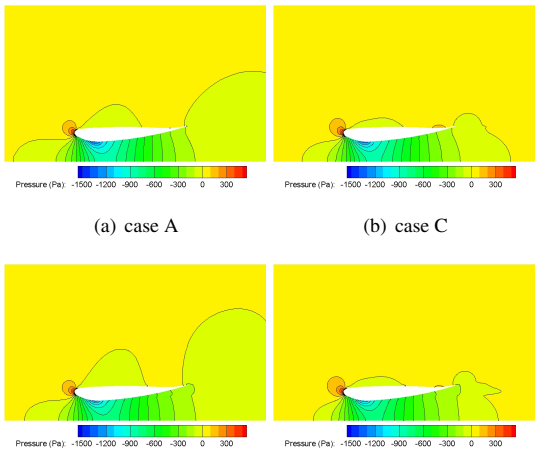

(a) case A (b) case C

(c) case B (d) case D

Figure 2. *Pressure contours on the plane of symmetry, for the wing at a Reynolds number of 4.54x10^5 and angle of incidence of 3.45^o. Cases A and B are in the body-stationary reference frame and cases C and D are in the body-moving reference frame. Cases A and C utilize the Realizable k-ε model and cases B and D utilize the RSM.*

for a wing in ground effect is seen from the significant increase in low pressure existing between the wing suction surface and the ground surface.

There are some small differences, however, between both the use of the turbulence model (cases A,C and cases B,D) and the use of the reference frame (cases A,B and cases C,D). These variations are seen particularly on the upper surface near the trailing edge, and in the suction peak on the lower surface. Taking case A as the baseline, case B varies in peak pressure by 7%, case C by 2% and case D by 11%.

Considering now the velocity contours on the symmetry plane in Figure 3, the use of the different reference frames is clear. Cases A and B are in the typical body-stationary reference frame, where the freestream velocity of 30 ms^{-1} is visible throughout most of the flowfield. The slow velocity wake is seen downstream of the wing and beneath the wing a high velocity region exists, which is noted as the cause of the pressure increase (and therefore increase in downforce).

In our earlier work (Close & Barber, 2014), we found that the representation of ground effect flowfields in a body-moving reference frame was beneficial in explaining the fluid dynamics producing the altered aerodynamic characteristics. The fluid is seen to be pushed forward at the leading edge, and then under the wing surface, where the high speed air cause the pressure change between the wing surface and the ground. In the wake region, the air is dragged along with the wing. A small region beneath the wing trailing edge experiences the flow moving both towards the leading edge, next to the wing surface, and away from the leading edge, in the region between the wing surface and the ground.

This is demonstrated in Figure 4, where the velocity on a line located along the symmetry plane and at a location 2/3 c from the leading edge is plotted. The abrupt change in velocity direction for the body-moving cases is seen, in

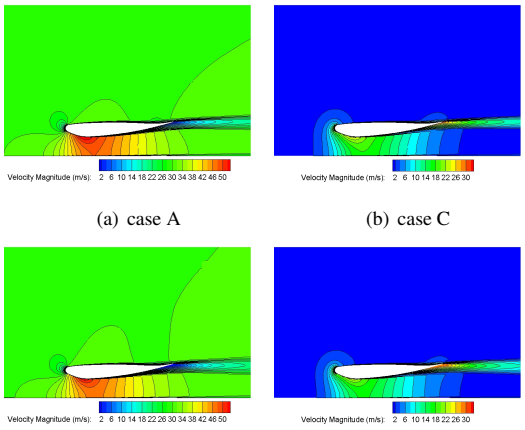

(a) case A (b) case C

(c) case B (d) case D

Figure 3. *Velocity contours on the plane of symmetry, for the wing at a Reynolds number of 4.54x10^5 and angle of incidence of 3.45^o. Cases A and B are in the body-stationary reference frame and cases C and D are in the body-moving reference frame. Cases A and C utilize the Realizable k-ε model and cases B and D utilize the RSM.*

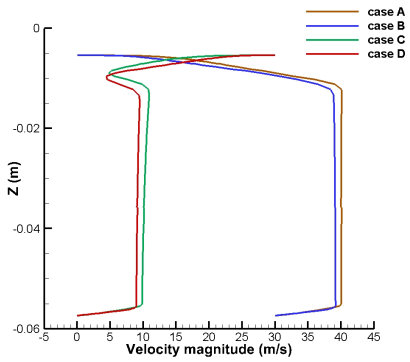

Figure 4. *Velocity on a line located along the symmetry plane and at a location 2/3 c from the leading edge. Cases A and B are in the body-stationary reference frame and cases C and D are in the body-moving reference frame. Cases A and C utilize the Realizable k-ε model and cases B and D utilize the RSM.*

contrast to the velocity curves for the body-stationary cases.

The effect of the velocity change on the generation of turbulence is seen in Figure 5. The region closest to the wing surface is shown here to highlight the variation between the four cases. Case A and C show negligible difference however a (very) small variation is observed between cases B and D. Given that these cases utilize the second order RSM closure, the existence of discrepancy due to curvature or flow history is more likely to be apparent and the turbulent production generated by the interaction with the mean flow is likely to be better represented. However given the magnitude of this difference it cannot conclusively be attributed to the reference frame variation.

Considering now the effects in the three-dimensional plane, the turbulence intensity is found on the ground plane.

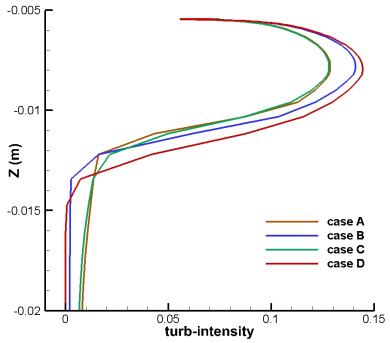

Figure 5. *Turbulence intensity on a line located along the symmetry plane and at a location 2/3 c from the leading edge (showing only the region closest to the wing surface for clarity). Cases A and B are in the body-stationary reference frame and cases C and D are in the body-moving reference frame. Cases A and C utilize the Realizable k-ε model and cases B and D utilize the RSM.*

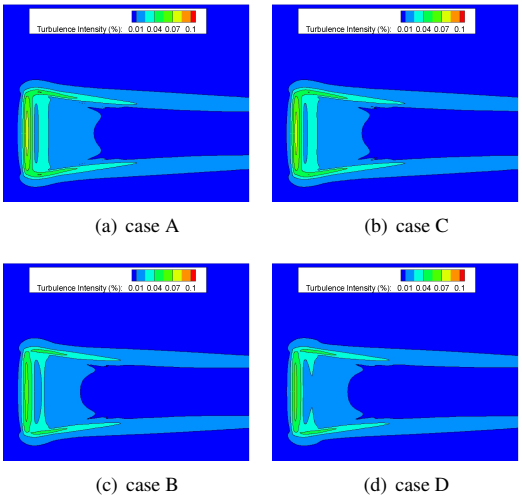

(a) case A (b) case C

(c) case B (d) case D

Figure 6. *Turbulence intensity contours on the ground plane, noting a symmetry plane reflection as been used for clarity. Cases A and B are in the body-stationary reference frame and cases C and D are in the body-moving reference frame. Cases A and C utilize the Realizable k-ε model and cases B and D utilize the RSM.*

While shear rates will be negligible for most regions of the moving ground - as the ground is either moving at the same speed as the air, or both ground and air are stationary - it was considered that the disturbed flow beneath the wing may contribute to a reference-frame induced flow-field variation. In Figure 6, negligible difference is found between the k-ε model cases, A and C. A small variation is seen for the RSM model cases, B and D, in the region beneath the wing. Again, this difference is very small, but it is significant that the variation has been observed only in the more accurate RSM model.

A further examination of the three-dimensional effects is seen in Figure 7, which displays the velocity magnitude

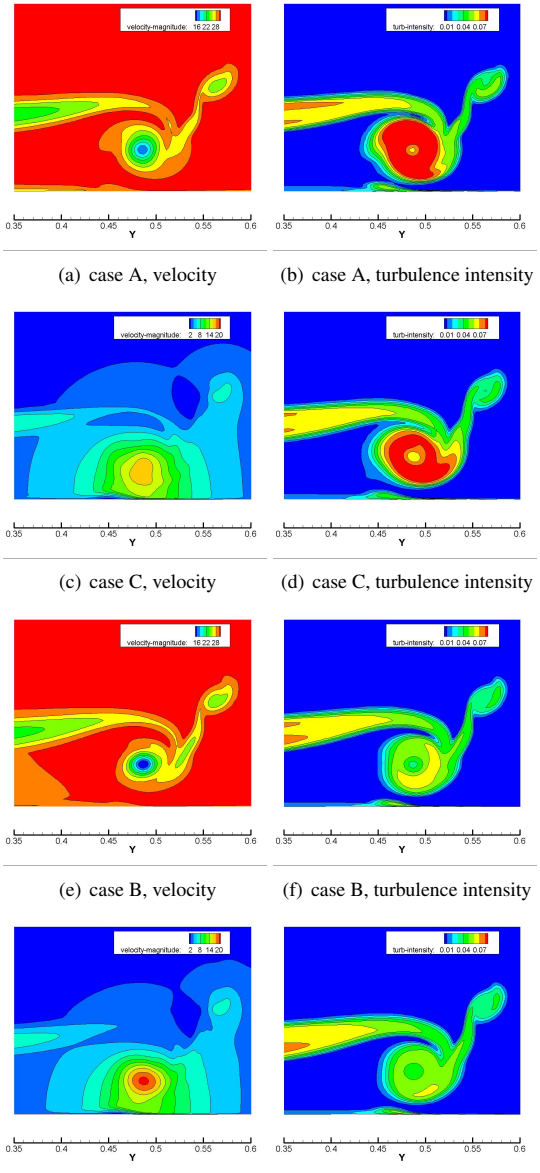

(a) case A, velocity (b) case A, turbulence intensity

(c) case C, velocity (d) case C, turbulence intensity

(e) case B, velocity (f) case B, turbulence intensity

(g) case D, velocity (h) case D, turbulence intensity

Figure 7. *Velocity and turbulence intensity contours on a plane 1 c downstream from the leading edge. Cases A and B are in the body-stationary reference frame and cases C and D are in the body-moving reference frame. Cases A and C utilize the Realizable k-ε model and cases B and D utilize the RSM.*

and turbulence intensity contours on a plane one chord-length downstream of the wing trailing edge. It is noted that some variation among all four cases, in these images where the vortex structure can be visualized (as is the viscous boundary layer beginning to form on the ground surface). The vortex structure forms off the edge of the endplate, with a primary vortex forming inside the endplate and a secondary vortex formed outside the upper edge of the endplate (Keogh *et al.*, 2015). In the body-moving models, the vortices are seen as regions of high speed air, with a very clear ground influence (which is not observed as clearly in

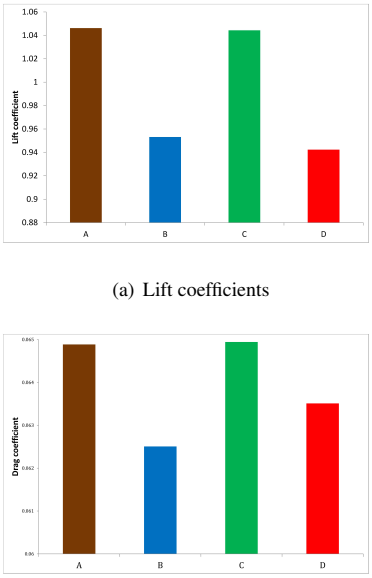

(a) Lift coefficients

(b) Drag coefficients

Figure 8. *Lift and drag coefficients for the four cases studied. Cases A and B are in the body-stationary reference frame and cases C and D are in the body-moving reference frame. Cases A and C utilize the Realizable k-ε model and cases B and D utilize the RSM.*

the body-stationary cases). The peak velocity varies between the turbulence models. The k-ε model predicts a higher level of turbulent flow within the vortex, however the overall shape is similar between the four cases. Both closure models show minor variation between the moving and stationary implementations.

There are some small differences to be noted in the force coefficients calculated for the four cases (Figure 8). It is not surprising to see some variation between the two closure models, but there is also a variation between the moving and stationary cases, however only for the RSM models. This result follows from the small variations noted in the flow field for the two cases, and it is expected that some discrepancy would be then noted in the integrated forces.

CONCLUSIONS

A comparison of moving and stationary reference frames was conducted for two RANS turbulence models, to determine any discrepancies that may arise from the numerical implementation of the turbulence present in each frame. In the stationary case, the wing is assumed to be in a body-stationary reference frame, such as in a wind tunnel situation. This framework is also used for CFD models of aerodynamic problems. The real-life case, of course, relates to a body-moving reference frame, in which the air is quiescent until disturbed by the wing. In a body-stationary problem, we introduce a non-physical level of turbulence into the oncoming air. In a moving ground problem, this non-physical disturbance is further compounded by the introduction of a moving surface along the lower boundary which will in turn generate additional turbulent (or unsteady) disturbances into the freestream.

Flow features in both reference frames were presented to demonstrate the difference in the flow field explanations that can occur, and this was highlighted for the region beneath the wing. Minor differences in results were found, for both velocity and turbulence parameters. Variation was found between turbulence models also, as expected.

While some variation in reference frame results may be attributed to the numerical solution and boundary conditions (which were necessarily variant between reference frames), the larger increase in discrepancy for the RSM datasets does suggest some reference frame origin for the error.

However all differences were of a very small value and unlikely to prove any difficulty in using the commonly implemented body-stationary situation. A further study making use of extreme ground effect (less than 5% clearance) is planned, to determine if the error grows in this type of condition.

ACKNOWLEDGEMENTS

The authors acknowledge the use of the Trentino High Performance Computing resource in the School of Mechanical and Manufacturing Engineering, University of New South Wales.

REFERENCES

Ahmed, Mohammed R, Takasaki, T & Kohama, Y 2007 Aerodynamics of a naca4412 airfoil in ground effect. *AIAA journal* **45** (1), 37–47.

Barber, TJ, Leonardi, E & Archer, RD 1999 A technical note on the appropriate cfd boundary conditions for the prediction of ground effect aerodynamics. *Aeronautical Journal* **103** (1029), 545–547.

Barber, T, Leonardi, E & Archer, RD 2002 Causes for discrepancies in ground effect analyses. *Aeronautical Journal* **106** (1066), 653–668.

Close, P & Barber, T 2014 Explaining ground effect aerodynamics via a real-life reference frame. In *Applied Mechanics and Materials*, , vol. 553, pp. 229–234. Trans Tech Publ.

Diasinos, S, Barber, TJ, Leonardi, E & Hall, SD 2005 The validation of a 2d cfd model for the implementation of a moving ground in a unsw wind tunnel. In *5th Pacific Symposium on Flow Visualization and Image Processing (PSFVIP5), Daydream Island, Australia*.

Doig, G, Barber, T & Diasinos, S 2014 Implications of compressibility effects for reynolds–scaled testing of an inverted wing in ground effect. *International Journal of Aerodynamics* **4** (3), 135–153.

Giacomelli, R 1930 The aerodynamics of leonardo da vinci, jr aeronaut. *Soc* **34**, 1016–1038.

Keogh, J, Doig, G, Diasinos, S & Barber, T 2015 The influence of cornering on the vortical wake structures of an inverted wing. *Proc. IMechE. Part D: Journal of Automobile Engineering*. **in press**.

Launder, BE, Reece, G Jr & Rodi, W 1975 Progress in the development of a reynolds-stress turbulence closure. *Journal of fluid mechanics* **68** (03), 537–566.

Launder, Brian E 1989 Second-moment closure: present and future? *International Journal of Heat and Fluid Flow* **10** (4), 282–300.

Lee, S-H & Lee, J 2013 Aerodynamic analysis and multiobjective optimization of wings in ground effect. *Ocean Engineering* **68**, 1–13.

Pillai, N, Anil, T, Radhakrishnan, A, Vinod, R, Zaid, Z, Jacob, A & Manojkumar, M 2014 Investigation on airfoil operating in ground effect region. *International Journal of Engineering & Technology* **3** (4), 540–544.

Qu, Qiulin, Jia, Xi, Wang, Wei, Liu, Peiqing & Agarwal, Ramesh K 2014 Numerical study of the aerodynamics of a naca 4412 airfoil in dynamic ground effect. *Aerospace Science and Technology* **38**, 56–63.

Qu, Q, Wang, W, Liu, P & Agarwal, R 2015 Airfoil aerodynamics in ground effect for wide range of angles of attack. *AIAA Journal* pp. 1–14.

Shih, Tsan-Hsing, Zhu, Jiang & Lumley, John L 1993 A realizable reynolds stress algebraic equation model. *Linthicum Heights, MD: NASA Center for AeroSpace Information,— c1993* **1**.

Wilcox, David C *et al.* 1998 *Turbulence modeling for CFD*, , vol. 2. DCW industries La Canada, CA.

Zerihan, J & Zhang, X 2000 Aerodynamics of a single element wing in ground effect. *Journal of Aircraft* **37** (6), 1058–1064.